

This copy is for your personal, non-commercial use only.

If you wish to distribute this article to others, you can order high-quality copies for your colleagues, clients, or customers by [clicking here](#).

Permission to republish or repurpose articles or portions of articles can be obtained by following the guidelines [here](#).

The following resources related to this article are available online at www.sciencemag.org (this information is current as of January 5, 2010):

Updated information and services, including high-resolution figures, can be found in the online version of this article at:

<http://www.sciencemag.org/cgi/content/full/282/5397/2254>

This article **cites 16 articles**, 4 of which can be accessed for free:

<http://www.sciencemag.org/cgi/content/full/282/5397/2254#otherarticles>

This article has been **cited by** 98 article(s) on the ISI Web of Science.

This article has been **cited by** 22 articles hosted by HighWire Press; see:

<http://www.sciencemag.org/cgi/content/full/282/5397/2254#otherarticles>

This article appears in the following **subject collections**:

Ecology

<http://www.sciencemag.org/cgi/collection/ecology>

22. K. W. Nordeen and E. J. Nordeen, *Behav. Neural Biol.* **57**, 58 (1992).
 23. M. L. Sutter and D. Margoliash, *J. Neurophysiol.* **72**, 2105 (1994).
 24. M. A. Wilson and B. L. McNaughton, *Science* **265**, 676 (1994); W. E. Skaggs and B. L. McNaughton, *ibid.* **271**, 1870 (1996).
 25. A. C. Yu and D. Margoliash, *ibid.* **273**, 1871 (1996).
 26. J. S. McCasland, *J. Neurosci.* **7**, 23 (1987); A. C. Yu and D. Margoliash, unpublished data.
 27. H. Sakaguchi and N. Saito, *Brain Res. Dev. Brain Res.* **62**, 223 (1991); J. A. Soha, T. Shimizu, A. J. Doupe, *J. Neurobiol.* **29**, 473 (1996); C. F. Harding, S. R. Barclay, S. A. Waterman, *ibid.* **34**, 329 (1998).
 28. D. Margoliash, *J. Neurobiol.* **33**, 671 (1997).
 29. All procedures were approved by an institutional animal care and use committee. Supported by grants from the Whitehall Foundation, NIH (NS25677), and the Brain Research Foundation. A.S.D. and A.C.Y. were supported by NIH predoctoral fellowships.

14 August 1998; accepted 6 November 1998

Microscale Nutrient Patches in Planktonic Habitats Shown by Chemotactic Bacteria

Nicholas Blackburn,* Tom Fenchel, Jim Mitchell

Are nutrients available to microbial communities in micropatches long enough to influence growth and competition? And what are the sources of such patches? To answer these questions, the swimming behavior of chemotactic bacteria in seawater samples was examined. Clusters of bacteria formed in conjunction with cell lysis and excretion by protozoa. These point sources of nutrients spread into spherical patches a few millimeters in diameter and sustained swarms of bacteria for about 10 minutes. Within that time, a large proportion of the nutrients was encountered by bacteria, chemotactic and nonchemotactic alike. Chemotaxis is advantageous for bacteria using patches over a certain size.

The existence of microscale nutrient patches in pelagic habitats has important implications for microbial ecology (1). Patches represent resources that are available within limited time and space. This creates situations that encourage competitive foraging, and elevated concentrations within patches increase transfer rates of nutrients into the food web. One line of evidence that patches exist is based on observations that a proportion of aquatic bacteria swim, an effort that is beneficial only in an inhomogeneous nutrient environment (2). The nature of targets for chemotactic bacteria has remained largely a matter of speculation, although bacterial chemotaxis is stimulated by organic and inorganic compounds. Interest has focused on algal exudation since the discovery of symbiosis between bacteria and species of terrestrial plants (3–5), but experimental evidence has been contradictory (4, 6). Point-source releases of nutrients have been suggested to result in patches that are consumed before dispersing to background levels (7). We attempted to resolve the question by direct observation of microbial communities.

Observations of seawater samples (8) revealed that clusters of bacteria continuously

formed and dispersed. Some sources of attractants were identified as the autolysis of a large microbe, such as an algal cell or a

protozoan (Fig. 1A). Other clusters formed without any visually distinct source (Fig. 1B). Various species of ciliates were often seen at the center of these clusters, which we assumed were related to the discharge of undigested organic matter and inorganic nutrients from food vacuoles (9). Other zooplankton excrete plumes of nutrients (10). Studies have focused mainly on the importance of these nutrient plumes for phytoplankton growth (10, 11), and conclusions have been largely negative. However, bacteria have 100 times the uptake potential of phytoplankton and are therefore potential key players in rapidly consuming dissolved nutrients from patches and transferring them into the food web.

The current model of bacterial chemotaxis is based on swimming behavior of the enteric bacterium *Escherichia coli* (12). Reports of different swimming behavior displayed by strains of marine bacteria (13) pose the question of whether the model is widely applicable. To test this, we studied swimming behavior of bacteria from seawater enrichments under conditions of low oxygen saturation (14), where they were observed to form clusters around algae producing oxygen (Fig. 1C). Motility patterns could be reproduced by simulations (Figs. 1D and 2). At an intermediate distance, the mean radial component of runs toward the source increased by a factor of 2.5. This local maximum was a result of an alignment phenomenon, where runs heading

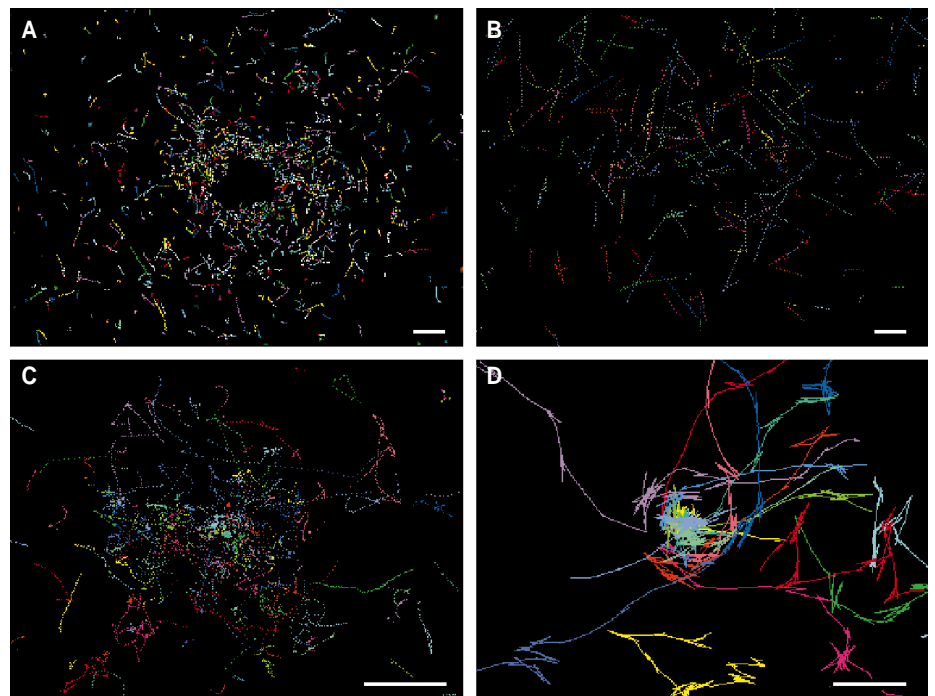


Fig. 1. (A) Cluster of bacteria around a lysed ciliate in a seawater sample tracked (21) over 2 s (velocity $v = 25 \mu\text{m s}^{-1}$, run duration $\tau = 0.3 \text{ s}$). (B) Cluster of large bacteria in a cloud of attractant in a seawater sample tracked over 2 s ($v = 50 \mu\text{m s}^{-1}$, $\tau = 0.5 \text{ s}$). (C) Bacteria cultured on 0.02% tryptic soy broth swarming around an individual *Pavlova lutheri* cell as a response to the oxygen gradient tracked over 16 s ($v = 25 \mu\text{m s}^{-1}$, $\tau = 0.3 \text{ s}$). (D) Simulation as described in Fig. 2 of the scenario shown in (C). Bars, 50 μm .

N. Blackburn and T. Fenchel, Marine Biological Laboratory, University of Copenhagen, Strandpromenaden 5, 3000 Helsingør, Denmark. J. Mitchell, School of Biology, Flinders University, Adelaide SA 5001, Australia.

*To whom correspondence should be addressed. E-mail: mblnb@mail.centrum.dk

up the gradient brought the bacteria quickly into a core zone. This is illustrated in Fig. 1D by the spokelike pattern surrounding the central zone of tight clustering. Reversal was important to chemotactic efficiency in this example: Decreasing the turn angle to 90° failed to reproduce visually obvious clusters. Run lengths decreased at close proximity to the attractant source where the probability of moving past it was high, resulting in the rapid initiation of reversal and run truncation. Run lengths down the gradient were quite constant in length (Fig. 2), as observed for *E. coli* (12).

The model of chemotaxis subsequently formed the basis for analysis of patches resulting from point-source releases of nutrients. Clusters of bacteria were observed to grow in size before subsiding within a few minutes (Fig. 3). The dissolved attractant for the chemotactic response was invisible, but spherical symmetry of clusters and their rate of dispersal indicated that they were the result of point-source releases of nutrients. When nutrients are released at a point, they spread rapidly into a spherical patch. The rate of spreading slows as the patch increases in size. A stationary bacterium in the proximity of such an event would find itself within a wave, which would peak sharply and disperse slowly. A chemotactic bacterium would begin to

move up the gradient as soon as it could detect its presence. This was simulated with a source of 1 pmol, which corresponds approximately to the dissolved free amino-acid pool in a cell of 10 μm in diameter (15). Again, the model was able to reproduce the response of the clustering phenomenon (Fig. 3), and allows the behavior of the cluster to be described in terms of the model. Thus, the pattern of response with time can be identified as a combined effect of molecular diffusion of the attractant, congregation of bacteria through the drift component of their movement, and their subsequent dispersal by the diffusive component of their movement. The pattern matched only that of an attractant of low molecular weight and correspondingly high diffusion coefficient; this fits a wide spectrum of inorganic and organic molecules including oxygen, sugars, nitrate, phosphate, and amino acids. The expected encounter of released matter over 10 min was 0.028% for nonmotile bacteria and 0.046% for chemotactic bacteria (Fig. 4), calculated by averaging the probability distributions. In this example, chemotactic bacteria would encounter, on average, 46% of their biomass within 10 min, if the patch contained 1000 bacteria equivalents of dissolved matter, and 10% of the population would encounter more than 100% (Fig.

4). Thus, patches offer a mechanism for supporting high bacterial growth rates independently of background concentrations. The phenomenon offers an explanation for why tracers originating from organism biomass can be assimilated by bacteria much more rapidly than when they are homogeneously distributed (16). The gain in nutrient exposure achieved by chemotaxis is dependent on the size of the patch. The gain was a factor 2 for a patch size of 1 pmol (Fig. 4), but it drops to 1 for 0.1 pmol and increases to 3.5 for 10 pmol (17). Bacterial chemotaxis is thus beneficial only under conditions where patches are of a certain size, unlike their importance for bacterial growth in general.

The patches illustrated by clusters in Fig. 1, A and B, were more than 1 mm in diameter, and the clusters contained over 1000 motile bacteria at concentrations up to 10⁷ ml⁻¹. Even background concentrations of bacteria (~10⁶ ml⁻¹) would significantly influence patch dynamics, and would ultimately result in their erosion by consumption. The estimates above indicate that dispersion and potential erosion time scales are similar (on the order of 10 min).

On this spatial and temporal scale, the effects of shear influence patch dynamics (18). At low oceanic shear rates of 0.005 s⁻¹, a patch would remain virtually undistorted, but it would be stretched into streamers at high shear rates. The importance of shear in the context of this study is difficult to evaluate. Firstly, shear is strongly intermittent (19), and secondly, by decreasing the concentration gradient, it decreases dispersion by molecular diffusion. Of particular importance to bacterial chemotaxis is the fact that shelter from shear exists during periods of low turbulence, during periods between bursts of turbulence, in habitats close to surfaces (for example, biofilms and large aggregates), and at boundaries such as thermoclines and pycnoclines.

Chemotactic bacteria have played the role of live probes in this study, showing the

Fig. 2. Analysis of the cluster shown in Fig. 1C containing 930 runs. Radial components of run lengths relative to the center of the source (single *P. lutheri* cell) are plotted as a function of distance, separated into those moving toward and away from the source (up and down the gradient). Run lengths were closely Poisson distributed. The corresponding simulation based on the standard model of chemotaxis (22) with the measured motility parameters of $v = 25 \mu\text{m s}^{-1}$ and $\tau = 0.3 \text{ s}$ is shown for comparison. The simulation was based on 20 individuals, swimming in the estimated steady-state oxygen gradient produced by the cell (23), over a time period of 1000 s.

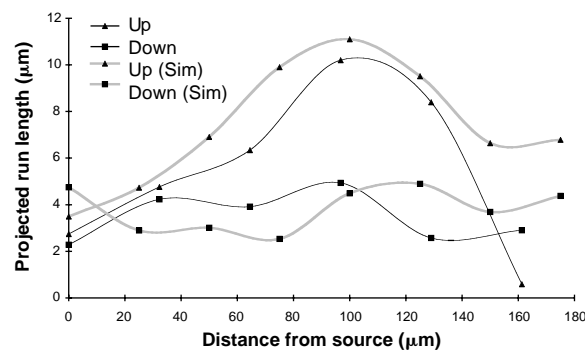


Fig. 3 (left). Normalized bacterial concentrations close to the lysed ciliate (Fig. 1A) within an area of 0.05 mm², and the cloud (Fig. 1B) within an area of 0.16 mm², are plotted with time. A simulation based on the standard model of chemotaxis (22) and a spreading patch (24) is shown for comparison. Bacterial concentrations in simulations were averaged over an area of 0.16 mm².

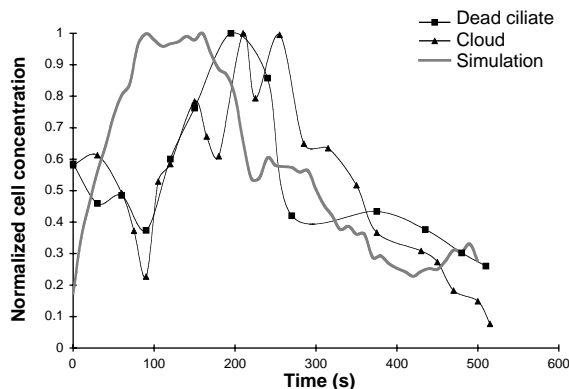
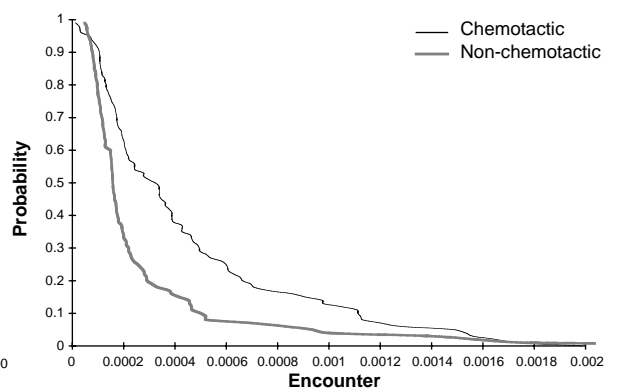


Fig. 4 (right). The probability of a bacterium encountering (25), within 10 min, a given proportion of the amount of

substrate in a spreading patch of size 1 pmol, comparing chemotaxis (as in Fig. 3) with nonchemotaxis (simulated by setting swimming velocity to 0).



dynamics of dissolved nutrient patches. We have yet to identify the frequency of occurrence and magnitude spectra of such patches in specific microbial food webs. They undoubtedly represent interesting ecological niches for bacteria, and they will also contribute much to our understanding of the flow of nutrients and energy in aquatic ecosystems if they prove to be major pathways.

References and notes

1. J. C. Goldman, *Bull. Mar. Sci.* **35**, 462 (1984).
2. E. M. Purcell, *Am. J. Phys.* **45**, 3 (1977).
3. G. A. Jackson, *Limnol. Oceanogr.* **32**, 1253 (1987).
4. W. Bell and R. Mitchell, *Biol. Bull.* **143**, 265 (1972).
5. J. G. Mitchell, A. Okubo, J. A. Fuhrman, *Nature* **316**, 58 (1985); J. D. Bowen, K. D. Stolzenbach, S. W. Chisholm, *Limnol. Oceanogr.* **38**, 36 (1993).
6. N. Blackburn, unpublished observations.
7. _____, F. Azam, Å. Hagström, *Limnol. Oceanogr.* **42**, 613 (1997).
8. Samples were taken, immediately before observation, from the vicinity of algal mats in a large seawater aquarium with high through-flow. The microbial community could be characterized as being rich and diverse. Identical communities have been observed in completely natural habitats. A standard microscope fitted with a dark-field condenser was used for observation with a 10× objective giving a depth of field of ~20 μm. The magnification was increased for some recordings with a magnifying lens. Samples were observed in a chamber made by a 1.5-mm-thick rubber O-ring placed on top of a microscope slide and covered with a cover slip. A fiber optic light source was used for illumination to minimize heat transfer. A standard video camera and VCR were used for recordings.
9. A. Andersson, C. Lee, F. Azam, Å. Hagström, *Mar. Ecol. Prog. Ser.* **23**, 99 (1985); P. A. Jumars, D. L. Penry, J. A. Baross, M. J. Perry, B. W. Frost, *Deep-Sea Res.* **36**, 483 (1989).
10. J. T. Lehman and D. Scavia, *Proc. Natl. Acad. Sci. U.S.A.* **79**, 5001 (1982).
11. P. J. L. Williams and L. R. Muir, in *Ecohydrodynamics*, J. C. J. Nihoul, Ed. (Elsevier, New York, 1981), pp. 209–218; D. J. Currie, *J. Plankton Res.* **6**, 591 (1984); G. A. Jackson, *Nature* **284**, 439 (1980).
12. D. A. Brown and H. C. Berg, *Proc. Natl. Acad. Sci. U.S.A.* **71**, 1388 (1974).
13. T. Fenchel, *Microbiology* **140**, 3109 (1994); J. G. Mitchell *et al.*, *Appl. Environ. Microbiol.* **61**, 877 (1995); J. G. Mitchell, L. Pearson, S. Dillon, K. Kantalis, *ibid.*, p. 4436; J. G. Mitchell, L. Pearson, S. Dillon, *ibid.* **62**, 3716 (1996); G. M. Barbara and J. G. Mitchell, *ibid.*, p. 3985.
14. Samples of seawater were enriched with 0.02% tryptic soy broth and left overnight, after which the culture contained strains of highly motile bacteria. Samples were sandwiched between a slide and cover slip after the addition of cells from a pure culture of *Pavlova lutheri*. A ring of bacteria around the air-water interface of the chamber indicated near anoxia inside the chamber.
15. P. A. Wheeler, in *Nitrogen in the Marine Environment*, E. J. Carpenter and D. G. Capone, Eds. (Academic Press, New York, 1983), p. 309.
16. F. Azam and J. W. Ammerman, in *Flows of Energy and Materials in Marine Ecosystems*, M. J. R. Fasham, Ed. (Plenum, New York, 1984), p. 345.
17. N. Blackburn, T. Fenchel, J. Mitchell, data not shown.
18. J. D. Bowen and K. D. Stolzenbach, *J. Fluid Mech.* **236**, 95 (1992).
19. L. Karp-Boss, E. Boss, P. A. Jumars, *Oceanogr. Mar. Biol. Annu. Rev.* **34**, 71 (1996).
20. H. C. Berg and D. A. Brown, *Nature* **239**, 500 (1972).
21. Video sequences were digitized to computer memory at 25 frames s⁻¹. The resulting digital film-strips were analyzed frame by frame for trajectories of movement by LabTrack (DiMedia, Kvistgaard, Denmark). Objects moving out of the plane of focus resulted in short tracks and were filtered out of the set of track vectors. Tumbles were detected at points

where changes in trajectory angle between two video frames exceeded 1 rad. Runs were defined as periods between tumbles.

22. The enteric bacterium *E. coli* swims in straight runs interspersed by tumbles (20). Positive taxis is achieved by lengthening runs when positive changes in concentration are detected over a period of time (12). The model refined by Brown and Berg states that the mean increase in run duration Δτ is proportional to the positive rate of change of attractant concentration

$$\Delta\tau = \frac{\alpha}{K_D} \frac{\partial C}{\partial t}$$

where C is concentration, K_D is a dissociation constant (100 μM), and α is a sensitivity constant (1000 s). Simulations were performed by allowing cells to move against a concentration field (3). Cells were moved a distance determined by their swimming velocity and heading angle from a physical location whose attractant concentration was C₁ to another location of concentration C₂, within each simulated time step dt. The change in mean run duration could thus be calculated as

$$\Delta\tau = \frac{\alpha}{K_D} \frac{C_2 - C_1}{dt}$$

Negative changes were ignored. Run durations are Poisson distributed (12). The probability of tumbling after each time step is dt/(τ + Δτ). The desired Poisson process was implemented with a random generator to decide whether or not to tumble after each time step. Tumbles were simulated as reversals, and a Brownian rotation of 1 rad s⁻¹ was introduced.

Swimming velocities and mean run durations were acquired from tracks of live cells.

23. The steady-state concentration field C(r) was calculated as

$$C(r) = \frac{E}{4\pi D \sqrt{r}}$$

where oxygen exudation rate E = 0.25 fmol s⁻¹ was estimated from light-saturated photosynthesis of a cell 4 μm in diameter. The diffusion coefficient D = 10⁻⁵ cm² s⁻¹. The inverse square-root dependency on the distance r from the source was introduced instead of inverse proportionality (3) to more closely approximate its shape in the flat chamber.

24. The concentration field C(r,t) of a spreading patch was calculated as

$$C(r,t) = M(4\pi Dt)^{-1.5} e^{-\frac{r^2}{4Dt}}$$

where M is the amount of matter released (1 pmol), and D = 10⁻⁵ cm² s⁻¹. Simulations were based on 100 individuals initially distributed randomly within a radius of 1 mm from the source. Velocity v = 50 μm s⁻¹, τ = 0.4 s.

25. The mass flow of a solute at concentration C with diffusion coefficient D toward a sphere of radius a is 4πaDC.

26. We thank the Swedish Foundation for International Cooperation in Research and Higher Education (STINT), the Danish National Research Council (SNF), the Australian Research Council, and Flinders University for support of this study.

12 June 1998; accepted 3 November 1998

Prevention of Population Cycles by Parasite Removal

Peter J. Hudson,* Andy P. Dobson, Dave Newborn

The regular cyclic fluctuations in vertebrate numbers have intrigued scientists for more than 70 years, and yet the cause of such cycles has not been clearly demonstrated. Red grouse populations in Britain exhibit cyclic fluctuations in abundance, with periodic crashes. The hypothesis that these fluctuations are caused by the impact of a nematode parasite on host fecundity was tested by experimentally reducing parasite burdens in grouse. Treatment of the grouse population prevented population crashes, demonstrating that parasites were the cause of the cyclic fluctuations.

Mathematical models have shown that a density-dependent response acting with a time delay can generate population cycles between natural enemies and their prey (1). Indeed, trophic interactions rather than intrinsic mechanisms are now considered by many to be the principal cause of cycles in microtine rodents (2), snowshoe hares (3), and red grouse (4). The definitive test of these hypotheses is to stop population cycles by manipulating the causative mechanism. Here, we report on a long-term, large-scale, replicated field experiment that examined the capacity of parasites to cause

cycles. The impact of the parasitic nematode *Trichostrongylus tenuis* on individual red grouse (*Lagopus lagopus scoticus*) was reduced through the application of an anthelmintic before a cyclic population crash in northern England.

Extensive investigations of hunting records from 175 individually managed grouse populations, coupled with detailed intensive demographic studies, have shown that 77% of red grouse populations exhibit significant cyclic fluctuations with a period between 4 and 8 years (Fig. 1A) (4). Population growth rate is negatively related to the intensity of worm infection in adult grouse (Fig. 1B), and poor breeding production is correlated with worm intensity (Fig. 1C), so that population crashes are associated with high parasite intensities. Analyses of parasite-host models predict that parasitic helminths can cause population cycles when they induce a reduction in host fecundity

P. J. Hudson, Institute of Biological Sciences, University of Stirling, Stirling FK9 4LA, UK. A. P. Dobson, Department of Ecology and Evolutionary Biology, Eno Hall, Princeton University, Princeton, NJ 08544–1003, USA. D. Newborn, Game Conservancy Trust, Swaledale, North Yorkshire DL8 3HG, UK.

*To whom correspondence should be addressed. E-mail: p.j.hudson@stir.ac.uk